STANDARDIZED REPRESENTATION OF LUNAR LOBATE SCARP TOPOGRAPHY - INITIAL RESULTS

P. Mahanti[1], J.D. Clark[1],T.R. Watters[2], M.E. Banks[2,3], M.S.Robinson[1] [1]Lunar Reconnaissance Orbiter Camera, School of Earth and Space Exploration, Arizona State University, Tempe, Arizona (pmahanti@asu.edu) [2]Center for Earth and Planetary Studies, National Air and Space Museum, Smithsonian Institution, Washington, D.C. [3]NASA Goddard Space Flight Center, Greenbelt, MD

Introduction: Lobate fault scarps (LS) are prevalent tectonic landforms across the lunar surface. They are the surface expressions of low-angle thrust faults formed by the contraction of the crust principally from long-term interior cooling [1, 2, 3, 4] and along with orbit recession and tidal deformation [5, 6, 7]. They are among some of the youngest landforms on the Moon ($<$ 1 Ga) based on their crisp appearance, absence of superposed craters, and model age estimates [4, 8, 9, 10, 11, 12]. The crisp morphologies and the survival of small (several to tens of meters width) graben on the back-limb of scarps suggest that many of the scarps have been active in the last 50 Ma, possibly even currently active [13, 14, 6]. Over 3500 lobate scarps have been identified on the Moon, ranging from up to $\sim$22 km in length and have a cross-sectional topographic maximum relief between $\sim$5 m and $\sim$150 m [15, 6].

Scarps have asymmetric profiles with a steeply dipping scarp face and a gently sloping back-limb. The topographic shape of the fault scarp cross section (LS profile hereafter), which varies across the length of the fault directly affects our understanding of the compressive (and extensional) kinematics that led to the lobate scarp morphology. The LS profile is defined by the geometric and kinematic properties of the fault, such as the depth of faulting, dip of the fault plane, and cumulative fault slip. To characterize the kinematic properties, measurements of topographic features from LS profile are required [5, 16]. For example, the relief (R) of the LS profile is related to the vertical displacement (D) which in turn is used to estimate the displacement length ($\frac{D}{L}$) ratio for the fault. A method that can robustly model the LS profile and is easily applicable across the entire fault length can offer significant advantages in the characterization of lobate scarps and would also provide additional constraints on forward mechanical models [5, 16].

Earlier work [17] has shown that elevation profiles of relatively smooth topographic features can be efficiently represented mathematically by Chebyshev approximation coefficients. For example, topography of nearly all lunar craters can be efficiently represented by only 17 Chebyshev coefficients [17]. In this representation, individual Chebyshev polynomial functions are scaled and summed to approximate the true elevation profile. The scaling factors are the Chebyshev coefficients which then represent the shape.

In this abstract, we propose a novel method for standardized representation of lunar lobate scarp topography. We will apply Chebyshev approximation here to encode lobate scarp shapes and discuss the efficiency and usefulness of the approximation process and the associated morphological correspondence of Chebyshev coefficients C_1 and C_2.

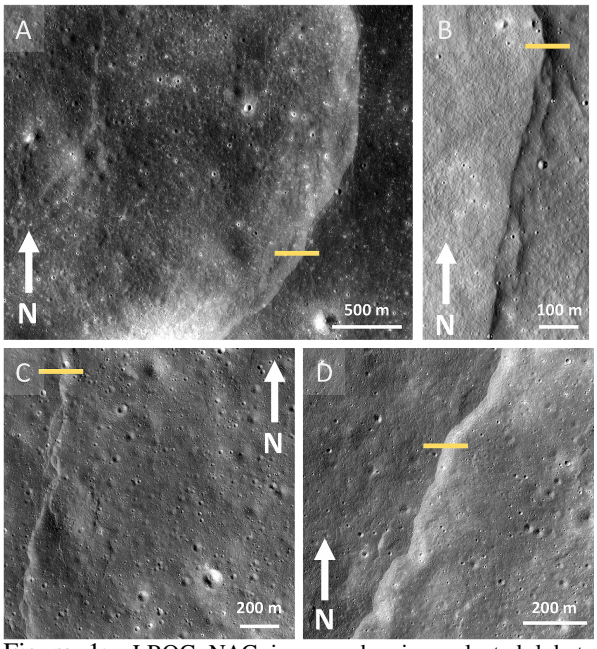

Figure 1: LROC NAC images showing selected lobate scarps (A) Racah X-1 (-10.1 N, 176.1 E; M143459779), (B) Mandel'shtam-6 (5.8 N, 161.5 E; M161252379), (C) Feoktiskov (32 N, 140.6 E, M; M151956846), and (D) Oppenheimer F (-34.2 N, -160.9 E; M151568945).

Methods: The four lobate scarp candidates chosen for this work were selected from a previous work [16] that compared digital terrain models (DTMs, derived from Lunar Reconnaissance Orbiter Camera stereo images) with generated fault dislocation models to better understand fault geometries. These four scarps were: Racah X-1, Mandel'shtam-6, Feoktiskov, and Oppenheimer F (Fig. 1).

Once the LS profiles were obtained (Fig.1; yellow line shows location), the Chebyshev coefficients are computed via the Chebyshev approximation (see [17] for details). The same topographic profile can be reconstructed using the Chebyshev coefficients and an entire topographic section can be reconstructed by this method which is then represented by fewer numbers (Fig. 2A). For this work, the order 'm' of the Chebyshev approximation was varied from 4 to 17 and the corresponding mean absolute error was computed for the entire eleva-

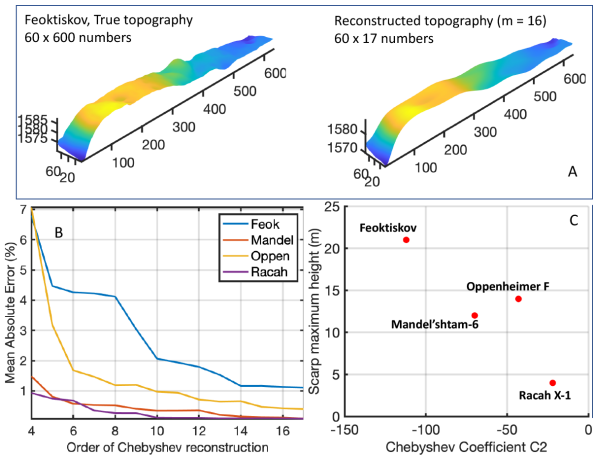

Figure 2: (A) Topographic section (60 adjacent profiles from the NAC DTM) of Feoktiskov reconstructed using Chebyshev approximation retains most of the shape (B) Variation of Mean absolute reconstruction error for the 4 lobate scarps with order of reconstruction (C) Scatterplot of estimated maximum scarp height vs. Chebyshev coefficient C_2

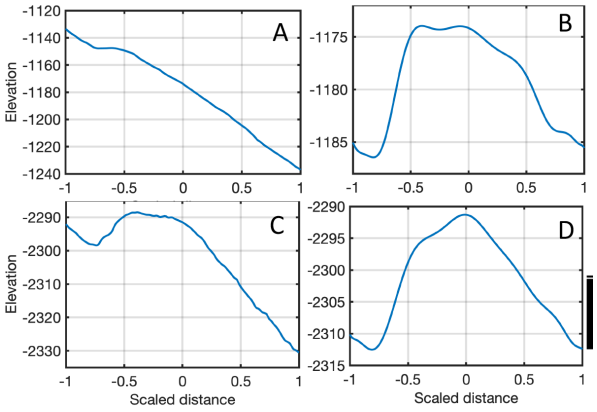

Figure 3: Elevation profiles for Mandel'shtam-6 and Oppenheimer F before (A and C) and after (B and D) slope detrending by setting coefficient C_1 to zero

tion profile to obtain an estimate of the reconstruction error (Fig. 2B). The maximum height of the scarp is compared with the third Chebyshev coefficient,C_2 (Fig. 2C) for all the scarps. The maximum height is estimated from the far-field slope-detrended topography obtained by reconstructing the profile from the approximated coefficients but setting the second Chebyshev coefficient C_1 to zero. Examples of slope detrending are shown for Mandel'shtam-6 and Oppenheimer F (Fig. 3).

Results and Discussion: Lobate scarps generally show smooth topography in cross-section and can be represented compactly by a small number of Chebyshev coefficients. Accordingly, when the order of reconstruction is increased above 12, the change in reconstruction error does not change significantly (Fig. 2B). By comparison, impact craters require a higher order of approximation (m = 16, 17 numbers are required for representing impact craters [17]).

The local relief for a scarp and the vertical fault displacement is not the same: $R > D$ for downhill-facing scarps, and $R < D$ for uphill-facing scarps depending on the dip of the surface [18]. Hence for either of these cases, the far-field slope has to be taken into account when estimating D [16, 18]. No additional step is required to estimate the far-field slope in the Chebyshev approximation process, and represented by the coefficient C_1. The sign of C_1 indicates whether the scarp is uphill or downhill facing.

The magnitude of Chebyshev coefficient C_2 is directly correlated to the maximum height of the scarp measured from the LS profile. Computation of C_2 does not require any additional steps to normalize the effects of far field slope and can be computed independently. Since the maximum height is directly related to $\frac{D}{L}$, C_2 normalized by the planimetric length L of the scarp can be used to classify scarps. Computation of C_2 at multiple points along the length of a scarp can provide additional knowledge about the growth of the scarp-related thrust fault by facilitating the construction of displacement profiles that provide insight into mechanical properties - a goal of our ongoing work.

Conclusion: We applied Chebyshev approximation to represent lobate scarp topography. Our results illustrate that the topographic shape of the lobate scarp can be efficiently represented by the Chebyshev approximation coefficients which capture the various aspects of the scarp shape. C_2, for example is strongly correlated (positive correlation) to the maximum vertical displacement of the fault scarp and hence the $\frac{D}{L}$ ratio. Future work will further explore this promising method in the context of a larger scarp database.

References: [1] Schultz P. H., *Moon morphology*, (1976). [2] Binder A. B. (1982) *The moon and the planets*, 26(2):117–133. [3] Watters T. R. et al., *Lunar tectonics*, *Cambridge University Press New York* (2010). [4] Watters T. R. et al. (2010) *Science*, 329(5994):936–940. [5] Watters T. R. et al. (2019) *Nature Geoscience*, 12(6):411–417. [6] Watters T. R. et al. (2015) *Geology*, 43(10):851–854. [7] Matsuyama I. et al. (2020) *Icarus*, 114202. [8] Binder A. B. and Gunga H.-C. (1985) *Icarus*, 63(3):421–441. [9] van der Bogert C. et al. (2012) (1847). [10] Clark J. D. et al. (2015) (1730). [11] van der Bogert C. H. et al. (2018) *Icarus*, 306:225–242. [12] Clark J. D. et al., (under review, submitted 2019). [13] Watters T. R. et al. (2012) *Nature Geoscience*, 5(3):181–185. [14] French R. A. et al. (2015) *Icarus*, 252:95–106. [15] Banks M. E. et al. (2012) *Journal of Geophysical Research: Planets*, 117(E12). [16] Williams N. et al. (2013) *Journal of Geophysical Research: Planets*, 118(2):224–233. [17] Mahanti P. et al. (2014) *Icarus*, 241:114–129. [18] Roggon L. et al. (2017) *Icarus*, 292:111–124.